Chemical Science

ROYAL SOCIETY OF CHEMISTRY

EDGE ARTICLE

View Article Online
View Journal | View Issue

Cite this: *Chem. Sci.*, 2020, **11**, 1964

All publication charges for this article have been paid for by the Royal Society of Chemistry

The cross-talk modulation of excited state electron transfer to reduce the false negative background for high fidelity imaging *in vivo*†

Ao Jiang,[ab] Yuxia Liu,[b] Guang Chen,*[ab] Yong Li[a] and Bo Tang*[a]

In practice, high fidelity fluorescence imaging *in vivo* faces many issues, for example: (1) the fluorescence background of the probe is bleached by the wide intensity scale of fluorescence microscopy, displaying an inherent false negative background (**FNB**); and (2) the dosage of the probe has to be increased to achieve sufficient intensity for *in vivo* imaging, causing a vicious cycle that exacerbates the **FNB**. Herein, we constructed a fluorophore (**F**)–electron donor (**D**)–electron regulator (**R**) system, and thereby developed a dual modulation strategy for the *de novo* design of high fidelity probes. Using cross-talk modulation, the probe allows: (1) enhanced **ESET** (excited state electron transfer) from **F** to **D**, which minimizes the inherent **FNB** based on synergistic **PET** (photo induced electron transfer); and (2) the inhibition of **PET** and weakening of **ESET** from **F** to **D** to maximize the reporting intensity to further reduce the **FNB**, which is additionally enhanced by an overdose of the probe. To test the implementation, we constructed a 7-hydroxy-2-oxo-2*H*-chromene-3-carbaldehyde (**HPC**) series of probes, with HPC (**F**) as the fluorophore, 2-hydrazinylpyridine, which was screened as an electronically adjustable donor (**D**), and electronic regulators (**R**). In particular, **HPC-7** and **HPC-8** provided cell/zebrafish imaging with negligible background even using the rather low fluorescence scale of microscopy (a region for revealing hidden background). Interestingly, with the specificity of **HPC** for reporting zinc, we achieved probe **HPC-5**, which possesses both an ultralow inherent **FNB** and optimal reporting intensity for tissue and *in vivo* imaging, enabling the *in vivo* imaging of zinc in mice for the first time. Under this high-fidelity mode, the fluorescence monitoring of zinc ions during the development of liver cancer in mice was successfully performed. We envision that the dual modulation strategy with the **F–D–R** system could provide a useful concept for the *de novo* design of practical probes.

Received 14th November 2019
Accepted 20th December 2019

DOI: 10.1039/c9sc05765j

rsc.li/chemical-science

Introduction

Molecular probes can exhibit a significant optical response towards analytes. Owing to their reactive specificity, timely reporting and biological affinity, molecular-probe-based fluorescence imaging techniques have been rapidly developed for biological monitoring, molecular medicine and even surgical navigation.[1–10] However, in the actual imaging, there are several problems that are usually neglected: (1) inherent false negative background (**FNB**): although the background seems to be dark, the real background fluorescence will be exposed when the intensity scale of microscopy is compressed (Scheme 1A). Obviously, the real background is covered by the wide intensity scale of microscopy. This problem causes interference in imaging analysis, especially in cells or aquatic organisms. (2) Enhanced **FNB** owing to a vicious cycle: owing to the unsatisfactory reporting intensity, an increased dose of the probe is required, which unfortunately leads to a vicious cycle as higher dose give a stronger **FNB**. Inevitably, the imaging may carry the aggravated **FNB**, meaning that the accuracy and sensitivity will be reduced, especially for *in vivo* imaging. Therefore, although large numbers of excellent probes have been developed,[11–14] developing a high fidelity probe to minimize **FNB** is of urgent need in practical analysis.

Over time, in the pursuit of accurate and sensitive imaging, researchers have developed many strategies,[9,15–17] including electron transfer, structure rotation, hydrophilicity tuning, fluorescence assembly, and so forth. As far as the technique is concerned, whatever the mechanism features, the electron behavior should be the essential factor for controlling the optical properties. It is our belief that modulating the electron transfer with a single mechanism is limited and the excited

[a]*College of Chemistry, Chemical Engineering and Materials Science, Key Laboratory of Molecular and Nano Probes, Ministry of Education, Collaborative Innovation Center of Functionalized Probes for Chemical Imaging in Universities of Shandong, Institutes of Biomedical Sciences, Shandong Normal University, Jinan 250014, P. R. China. E-mail: chenandguang@163.com; tangb@sdnu.edu.cn*

[b]*The Key Laboratory of Life-Organic Analysis; Key Laboratory of Pharmaceutical Intermediates and Analysis of Natural Medicine, College of Chemistry and Chemical Engineering, Qufu Normal University, Qufu 273165, P. R. China*

† Electronic supplementary information (ESI) available. See DOI: 10.1039/c9sc05765j

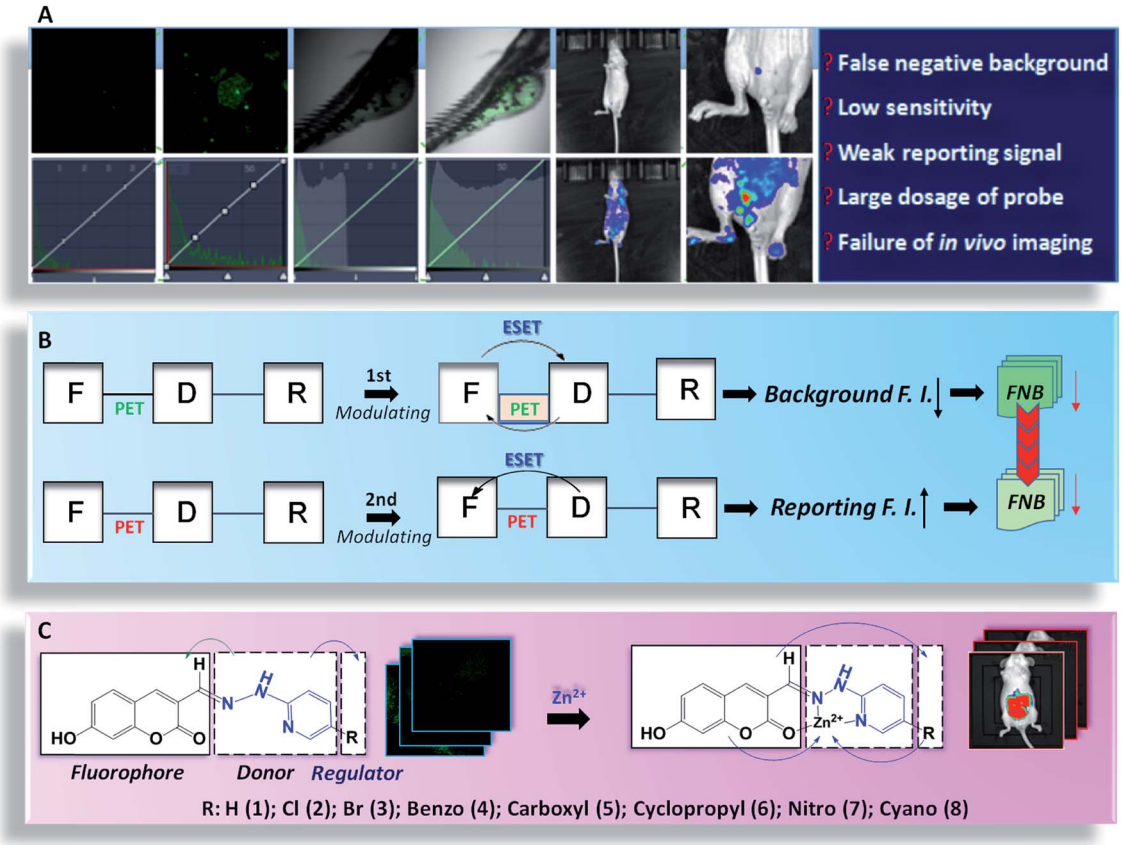

Scheme 1 (A) Some challenging barriers for practical imaging. (B) The working principle of the fluorescent fluorophore (F)–electron donor (D)–electron regulator (R) system. (C) The *de novo* design of the HPC series of probes.

state electron transfer (**ESET**) may be far beyond the control of a single factor. Thus, multiple factor cross-talk modulation may provide more preferable optical properties: (1) for light-penetrable samples, such as cells and aquatic organisms, the inherent false negative background fluorescence should be minimized; and (2) for samples with a poor transmittance, such as medical mice, the intensity of the reporting signal should be maximized, to reduce the dosage and thereby minimize the

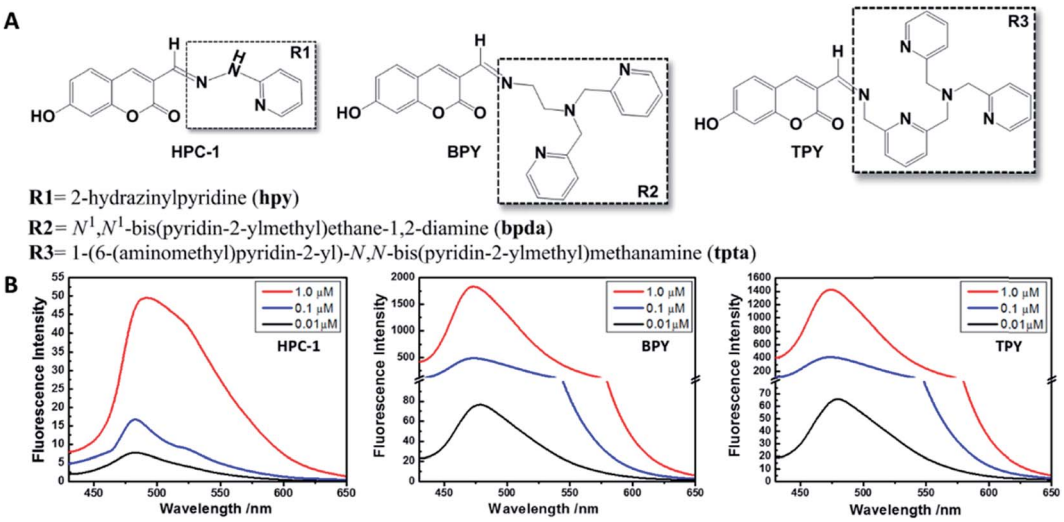

Fig. 1 (A) The structures of **HPC-1**, **BPY** and **TPY**. (B) Intensities from fluorescence background experiments involving probes **HPC-1**, **BPY** and **TPY** (0.01, 0.1, and 1 μM). All experiments were performed in HEPES buffer solution (50 mM HEPES, 100 mM KNO_3, pH = 7.2).

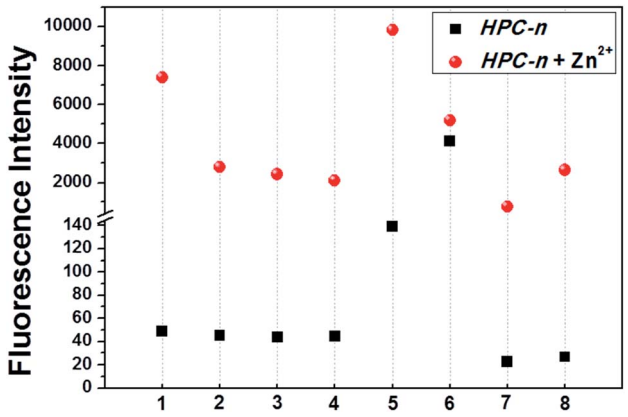

Fig. 2 The intensities of the fluorescence background (black squares) and reporting experiment (red circles) signals for HPC-*n* (*n*: 1–8) (1 μM) in response to Zn ions (20 μM). All experiments were performed in HEPES buffer solution (50 mM HEPES, 100 mM KNO_3, pH = 7.2).

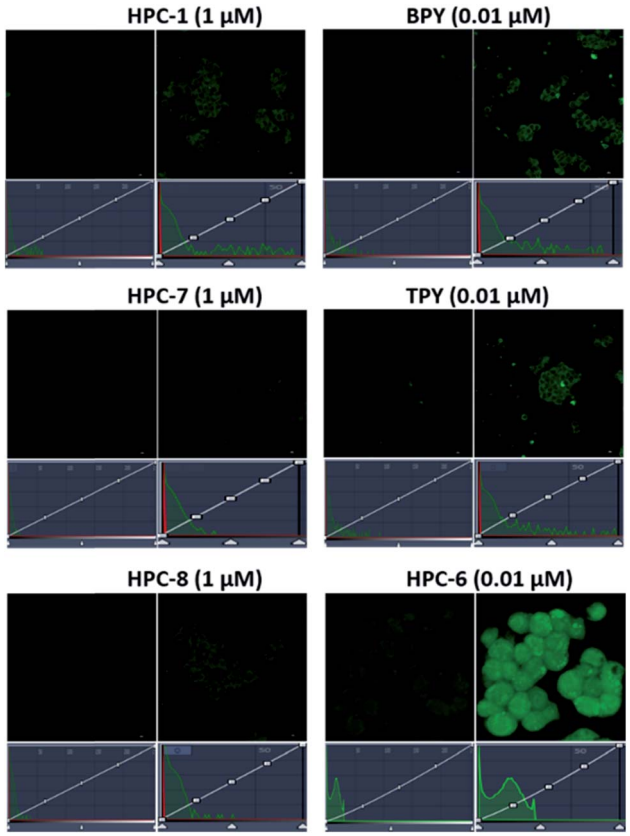

Fig. 3 Revealing the false negativity in the background of cell imaging hidden under the normal intensity scale of a fluorescence microscope. Hek293t cells pre-treated with TPEN (50 μM) were incubated with HPC-*n* (*n*: 1, 6, 7, 8), BPY and TPY for 20 min at 37 °C.

FNB. Therefore, developing the practical probe is a challenge, not only to improve the signal-to-noise ratio, but also to modulate the optical properties towards high fidelity imaging.

High fidelity imaging is critical for biomedical research, especially in tumor development. Zinc ions act as the essential contributor for tissue development.[18] In malignant tumors, zinc has been suspected to be associated with the developmental stages.[19–21] Although many excellent zinc probes have been developed,[22–35] there is still no research on *in vivo* imaging of Zn ions, which limits deeper insights into tumor development.

Accordingly, we constructed a system of a fluorophore (**F**)–electron donor (**D**)–electron regulator (**R**), and established a dual modulation strategy for the *de novo* design of high-fidelity imaging probes based on the cross-talk effect of **ESET** and photo induced electron transfer (**PET**). **F–D–R** worked as follows: (1) ensuring **PET** for fluorescence quenching and adjusting **R** for enhanced **ESET** from **F** to **D**, to minimize the **FNB**; and (2) inhibiting **PET** for fluorescence restoration and decreasing the **ESET** from **F** to **D**, to enhance the fluorescence, thereby further minimizing the **FNB**. For the implementation, we synthesized 7-hydroxy-2-oxo-2*H*-chromene-3-carbaldehyde (**HPC**)-*n* series probes, consisting of the fluorophore 7-hydroxy-2-oxo-2*H*-tryptone-3-acetaldehyde (**F**), an adjustable electron-rich donor 2-hydrazinopyridine (**D**), as well as the electronic regulators (**R**). Benefitting from this strategy, the **FNB** fluorescence became negligible even when the intensity scale of microscopy was drastically compressed, which significantly improved the authenticity and accuracy, as well as the sensitivity. For the application, with the specific response of **HPC**-*n* to zinc, the accumulation of zinc during tumor development was visualized. We anticipate this strategy can be applied to *de novo* design to optimize fluorescent probes for practical use.

Results and discussion

De novo design of probes for cells and zebrafish imaging

We selected **HPC** to be the fluorophore as it is easily influenced owing to its rich electrons and small planar structure. Furthermore, if we can quench it effectively then we can achieve an ultra-strong response. At the beginning, two classical groups **R2** (*N*1,*N*1-bis(pyridin-2-ylmethyl)ethane-1,2-diamine) (bpda) and **R3** (1-(6-(aminomethyl)pyridin-2-yl)-*N*,*N*-bis(pyridin-2-methyl)methanamine) (Fig. 1) were linked to **HPC** as the ideal design. As expected, the resultant probes **BPY** and **TPY** exhibited an excellent response to zinc ions. Unfortunately, the fluorescence background of these are strong, and increases sharply with the rising concentration (Fig. 1). These unsatisfactory results drove us to investigate the mechanism (Fig. 4). The density functional theory (DFT) calculation shows that the highest occupied molecular orbital (HOMO) energies of the two electron donors **R2** and **R3** are both much higher than that of the fluorophore **HPC**, indicating their conformation to the **PET** principle. Thus, **PET** alone is not sufficient to completely quench the fluorescence. Moreover, cell imaging also revealed that even at a very low dosage (0.01 μM), we still observed a significant **FNB** (Fig. 3). Under the default ruler of the fluorescence intensity (**BPY**: left column), the cells did not show a background. However, darkness in the imaging picture does not mean no fluorescence, while the **FNB** may be concealed by the default ruler of intensity. In fact, when the ruler is compressed to the low region (**BPY**: right column), even at only half of the default ruler, the **FNB** became significant.

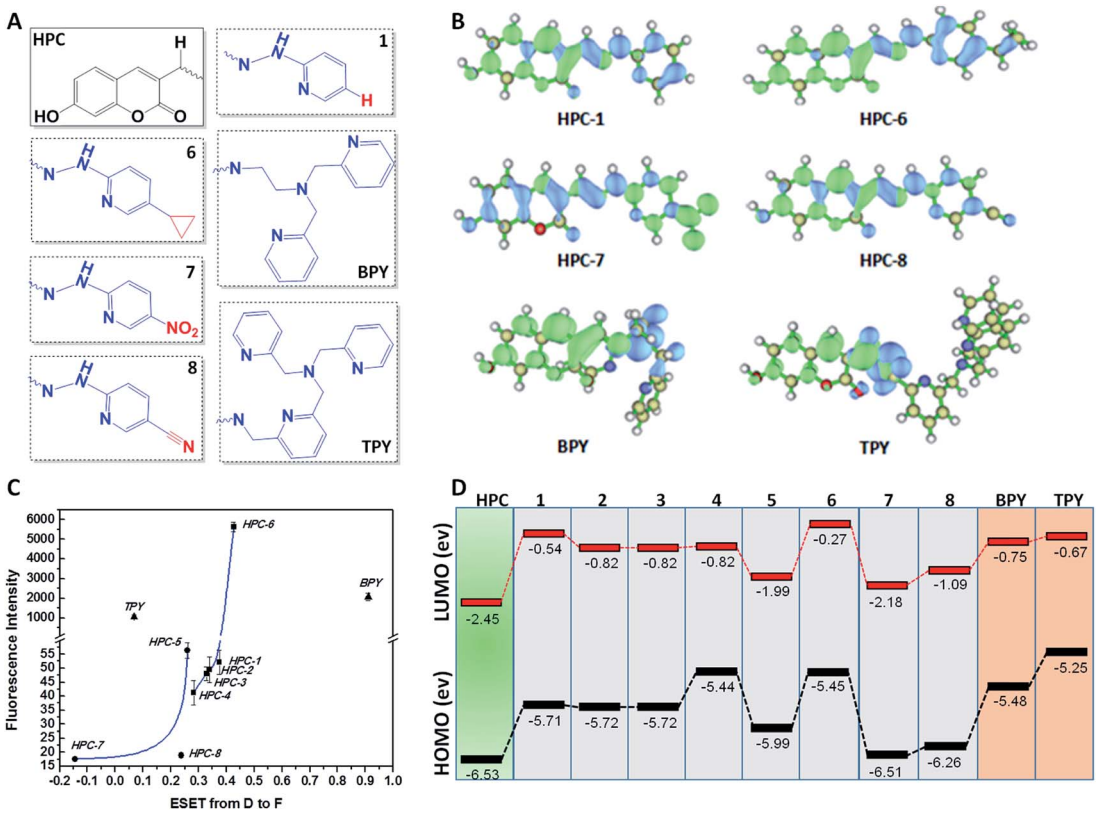

Fig. 4 (A) The structures of HPC-*n* (*n*: 1, 6, 7, 8), HPC, BPY and TPY. (B) Theoretical calculations of excited state electron transfer (green and blue represent the high and low electron densities, respectively). (C) ESET in the HPC-*n*, HPC, BPY and TPY structures. (D) The HOMO and LUMO orbital energies of HPC-*n*, HPC, BPY and TPY.

Consequently, although **BPY** and **TPY** have already conformed to the **PET** mechanism, their quenching effects are limited. These results lead us to suppose that, in addition to the pre-designed **PET**, if another modulating mechanism was introduced, further reduction of the fluorescence may be possible. Therefore, we set out to construct a cross-talk electronic modulation of **PET** and **ESET**. Discarding the classical **R2** and **R3**, we screened a moiety 2-hydrazinylpyridine (**hpy**) as it possessed both a high electron density and a planar conjugated structure for electron regulation. Firstly, we synthesized **HPC-1** in order to perform a preliminarily test for such a concept. As Fig. 1 indicates, when the concentration is 1.0 μM, the fluorescence intensity is 50, which is actually lower than that of **BPY** and **TPY** at 0.01 μM, demonstrating its powerful effect in reducing **FNB**. When **HPC-1** is reduced to 0.01 μM, the background intensity is rather low. These results indicate that introduction of the rich electron donor **hpy** into the fluorophore **HPC** is effective. Investigation of the electron configuration shows that, in **HPC-1**, the electrons of **hpy** are remarkably transferred to the orbital of **HPC** (Fig. 4B). In contrast, in **BPY** and **TPY**, the electronic contribution to **HPC** is not significant owing to their non-planar structures. Thus, it is promising to use **hpy** for effective multi-modulation of the electronic behaviour. However, although **HPC-1** exhibited an excellent quenching effect, in the imaging analysis, the **FNB** emerged when the intensity scale was compressed (Fig. 3). Thus, we set out to artificially interfere with the **ESET** for further control of the fluorescence intensity owing to the uneven electron distribution of the electron. Actually, in **BPY** and **TPY**, we found that the enhanced fluorescence intensity correlated with the increased **ESET** from **F** to **D** (Fig. 4C). Unfortunately, owing to the non-conjugated structures of these two, it is difficult to modulate the **ESET** in **BPY** and **TPY**. While in **hpy**, we can construct the system of **F–D–R** to cross-talk interfere with the electron transfer. With this in mind, we designed a series of **HPC-*n*** probes. As shown in Fig. 4D, the HOMO energies of these three groups are higher than those of **HPC**, indicating that they have met the basic requirements of **PET**. As expected, their fluorescence intensity is significantly different (Fig. 2), **HPC-7** and **HPC-8** exhibit quite a weak intensity, while **HPC-6** exhibits a very strong intensity, although it fully conforms to **PET**. Obviously, there is another electronic factor to give optical control in addition to **PET**. Then, we calculated the electronic distribution at the excited state to investigate the **ESET**. As indicated in Fig. 4C, **HPC-7** exhibits an **ESET** of 0.1443e from **HPC** to **hpy**, while **HPC-8** and **HPC-6** exhibit the opposite **ESET** of 0.2372 and 0.4265, respectively. These results indicated, in the excited state, that the electron transfer from **F** to **D** regulated by **R** reduced the electron density on **HPC**, thereby weakening the fluorescence intensity. Moreover, the excited state molecular orbitals were studied. Fig. 4B showed that in **HPC-7**, a remarkable electron transfer from **HPC** to **hpy** was observed. As

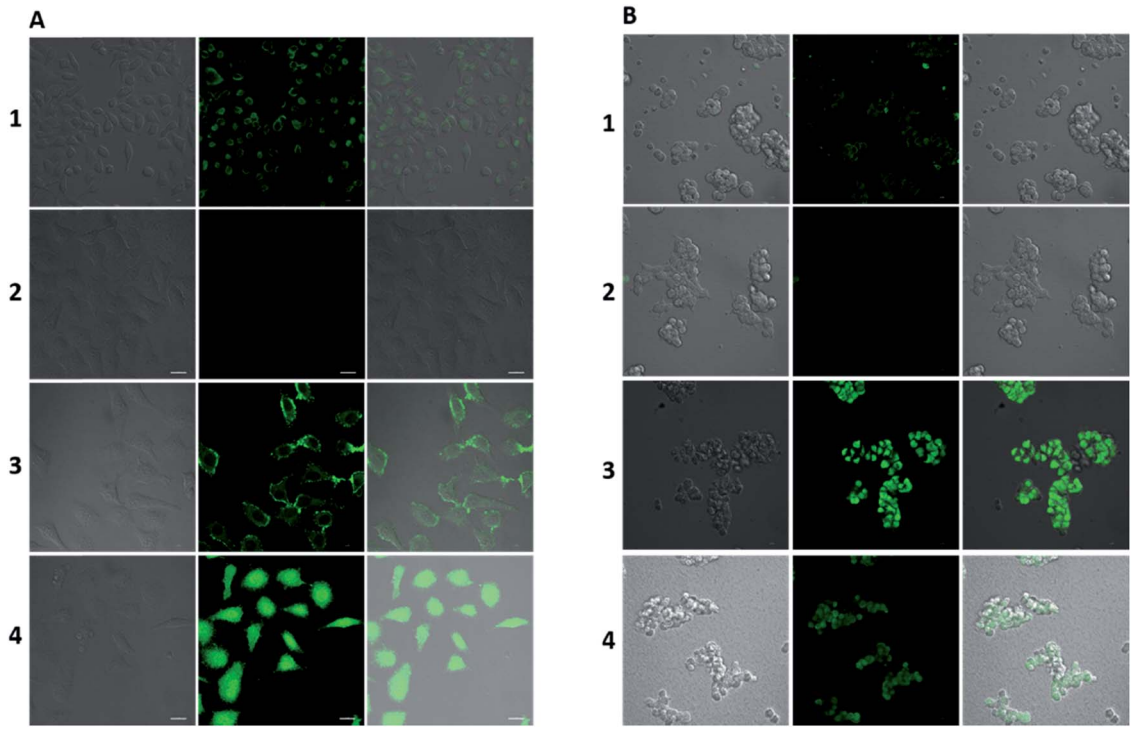

Fig. 5 Ultra-sensitive imaging of zinc in cells. (A) (1) SHSY-5Y cells treated with HPC-7 (1 μM) for 20 min. (2) SHSY-5Y cells pretreated with TPEN (50 μM) before incubation with HPC-7 (1 μM) for 20 min. (3) SHSY-5Y cells pretreated with Zn ions (10 μM) and a group of cells parallel to (2) for 20 min. (4) SHSY-5Y cells pretreated with Zn ions (50 μM) and a group of cells parallel to (3) for 20 min. (B) (1) Hek293t cells were treated with HPC-8 (1 μM) for 20 min. (2) Hek293t cells were treated with HPC-7 (1 μM) for 20 min. (3) Hek293t cells were pretreated with H_2O_2 (200 μM) for 5 h, then treated with HPC-8 (1 μM). (4) Hek293t cells were pretreated with H_2O_2 (200 μM) for 5 h, then treated with TPEN (50 μM) for 0.5 h, and then treated with HPC-8 (1 μM) for 0.5 h. Images are displayed under the compressed intensity scale of microscopy as in Fig. 3. Emission window: (left) bright field; (middle) green channel (430–650 nm); and (right) merged. Scale bar: 20 μm.

a result, the low electron density reduced the probability of the electronic transition, thereby leading to the weak fluorescence. Thus, cross-talk modulation of **ESET** and **PET** can be used to find an optimal probe. Then, we screened a series of groups as regulators and calculated their **ESET** (Fig. 4C). As can be seen, with the decreasing **ESET** from **HPC** to **hpy**, the fluorescence intensity decreased correspondingly. With this relationship, we can achieve an ultra-low background probe for cells and zebrafish imaging. As shown in Fig. 3, **HPC-6** still brings about a strong false negative background under the wide intensity scale, even when diluted to 0.01 μM. In sharp contrast, 1 μM of **HPC-7** and **HPC-8** exhibit a quite low fluorescence background even when the images were shown under the rather low intensity scale. Therefore, **HPC-7** and **HPC-8** can be used to minimize the **FNB** for high fidelity imaging. As an additional benefit, the compressed scale of intensity may contribute to more sensitive imaging than the default mode, as the intensity difference in the microscopic view becomes smaller under the compressed scale of intensity.

Ultralow FNB and high fidelity imaging in cells and zebrafish

Before analysis, we investigated the practicability of **HPC-7** and **HPC-8**, because although the two have a very low background, their responses to Zn ions may be different, which will alter their practical behaviors. At three levels (0.01, 0.1 and 1 μM), we tested their fluorescent responses toward Zn. As Fig. 7D shows, although **HPC-7** has a lower background, its responses are 9–52 fold, while **HPC-8** has a higher background, but better responses at 27–130 folds. We then performed imaging experiments using both of the two probes. All of the fluorescence intensity scales were set as the compressed region, as in Fig. 3. First, we used **HPC-7** to image the SHSY-5Y cells, as this probe had a lower fluorescence background while the SHSY-5Y cell contained more Zn.[36] As shown in Fig. 5A-1, the spontaneous zinc ions were visualized clearly using this probe. In parallel, the zinc chelator TPEN ((2-pyridylmethyl)ethylenediamine) was used to pre-treat cells before incubation with **HPC-7**. As shown in Fig. 5A-2, there was no background interference even under the very narrow intensity scale of the microscope, which was obviously attributed to the ultra-low background of **HPC-7**. Moreover, comparison of these two groups demonstrated that the fluorescence intensity in group 1 was triggered by the spontaneous zinc in the cells. To further confirm this result, we supplemented Zn ions to cells parallel to group 2. As shown in Fig. 5A-3, the fluorescence intensity increased significantly. With the increasing addition of Zn, an enhanced fluorescence intensity was observed (Fig. 5A-4), which confirmed that all of the fluorescence intensity in group 1 was triggered by the Zn ions without any interference from the fluorescence background. Furthermore, under the compressed intensity scale of

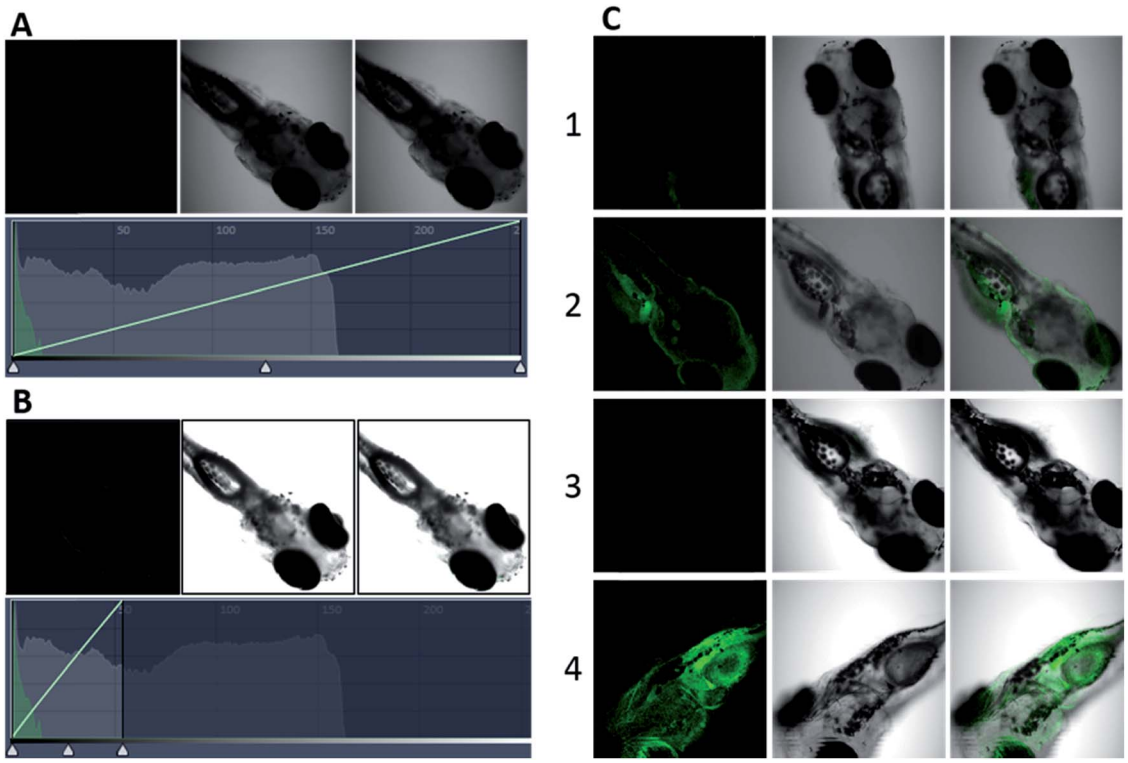

Fig. 6 Ultra-sensitive imaging of zinc in zebrafish. Zebrafish pretreated with TPEN (50 μM) for 60 min, then treated with **HPC-8** (1 μM) for 30 min: (A) under a normal scale of intensity; (B) under a compressed scale of intensity as indicated by the white triangle on the bottom. Zebrafish pretreated with TPEN (50 μM) for 60 min then treated with **HPC-8** (1 μM) for 30 min (C1)/(C3); zebrafish pretreated with **HPC-8** (1 μM) for 30 min (C2)/(C4): (C1) and (C2) under a normal scale of intensity; and (C3) and (C4) under a compressed scale of intensity, as in (B). Emission window: (left) green channel (430–650 nm); (middle) bright field; and (right) merged.

microscopy, the heterogeneous distribution of Zn ions can be observed (Fig. 5A-3), which is an additional benefit of the high fidelity imaging. Compared with the SHSY-5Y cells, the Hek293t cells contain less Zn ions.[37] Thus, we used **HPC-8** to image them as this probe possessed a higher sensitivity and stronger reporting intensity. It was found that although this probe responded, its intensity was not high owing to the low level of zinc in the Hek293t cells (Fig. 5B-1). Then, we used **HPC-7** as a control (Fig. 5B-2) and found that under the same intensity scale, the cells do not show observable imaging, indicating that **HPC-8** is more competent for imaging a reduced amount of analyte. Thus, we used **HPC-8** to image the zinc released by the apoptotic Hek293t cells. As shown in Fig. 5B-3, the H_2O_2-induced apoptotic cells showed an obviously enhanced fluorescence. To verify this result, TPEN was used. As shown in Fig. 5B-4, despite being apoptotic, caused by H_2O_2, the TPEN-treated cells showed a significantly weakened fluorescence intensity. Applications in different cells indicated the necessity to optimize the probe for high fidelity imaging analysis, which can be provided by the cross-talk modulation of electron transfer.

Next, we performed imaging analysis in zebrafish. Before the analysis, we investigated the fluorescence background of probes in zebrafish. We used 1 μM of **HPC-8** to incubate the TPEN-pretreated zebrafish. As shown in Fig. 6A, **HPC-8** in zebrafish exhibits a rather low fluorescence under the normal scale of intensity. Even if we compressed the scale to 20%, we did not find any fluorescence interference (Fig. 6B). Actually, from the fluorescence distribution, we can see that the strongest distribution is no more than 5% of the fluorescence scale, demonstrating the satisfactorily low background. Therefore, **HPC-8** was proven to be very suitable for high fidelity imaging of zebrafish. Owing to this property, we performed the following imaging analysis. Firstly, two groups of zebrafish were cultured with **HPC-8**, respectively, before and after TPEN treatment. Compared with the Fig. 6C-1 group, Fig. 6C-2 shows a strong fluorescence that reflects the spontaneous zinc ions in zebrafish. Next, we compressed the intensity scale to the same extent as that of Fig. 6B. As a result, Fig. 6C-3 showed no **FNB** and Fig. 6C-4 provided bright fluorescence images. Thus, **HPC-8** can provide highly accurate and sensitive imaging in zebrafish with negligible **FNB**. The above described studies demonstrate that an ultra-low background probe can be achieved by enhancing the **ESET** based on synergistic **PET**. Next, we applied this cross-talk strategy to image higher animals, such as mice. Thus, we investigated control of the reporting intensity using this strategy.

Cross-talk modulation of ESET and PET for *in vivo* imaging

According to the regulator, we divided the probes into three groups. First, we can see that both Zn–**BPY** and Zn–**TPY** show

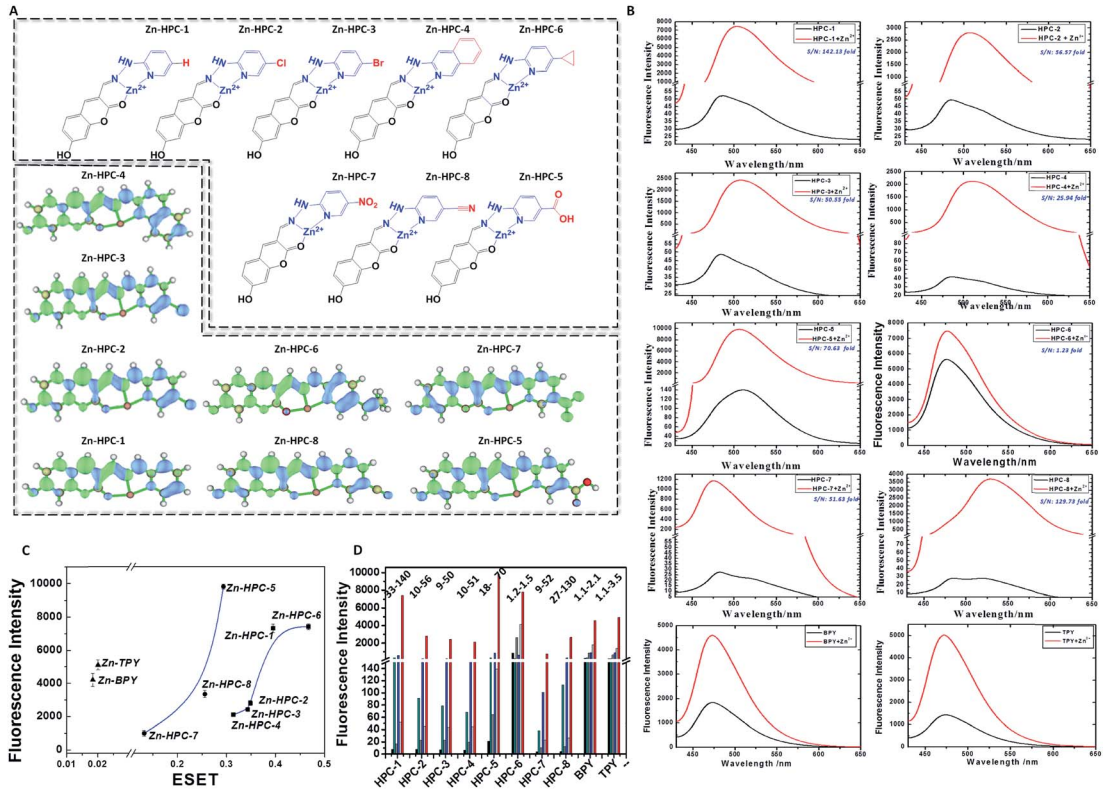

Fig. 7 (A) Structures and **ESET** (green and blue represent high and low electron densities, respectively) of Zn–**HPC**-*n* (*n*: **1**–**8**) in the excited state. (B) Fluorescence intensity changes of **HPC**-*n* (*n*: **1**, **6**, **7**, **8**; 1 μM), **BPY** (1 μM) and **TPY** (1 μM) in response to Zn ions (20 μM). (C) **ESET** in Zn–**HPC**-*n* (*n*: **1**–**8**). (D) Fluorescence response of **HPC**-*n* (0.01; 0.1; and 1 μM), **BPY** (0.01; 0.1; and 1 μM) and **TPY** (0.01; 0.1; and 1 μM) to Zn ions (20 N). Experiments were performed in HEPES buffer solution (50 mM HEPES, 100 mM KNO_3, pH = 7.2).

a weak **ESET** from the donor to **HPC** (Fig. 7C). Correspondingly, the fluorescence intensities of these are not strong. Moreover, the fluorescent enhancement was only 2.1–3.5 fold (Fig. 7D) with a strong **FNB**. Thus, **BPY** and **TPY** were far from meeting the requirements for imaging. The second group includes **HPC-1**, **HPC-2**, **HPC-3**, **HPC-4** and **HPC-6**, and shows significant **ESET**

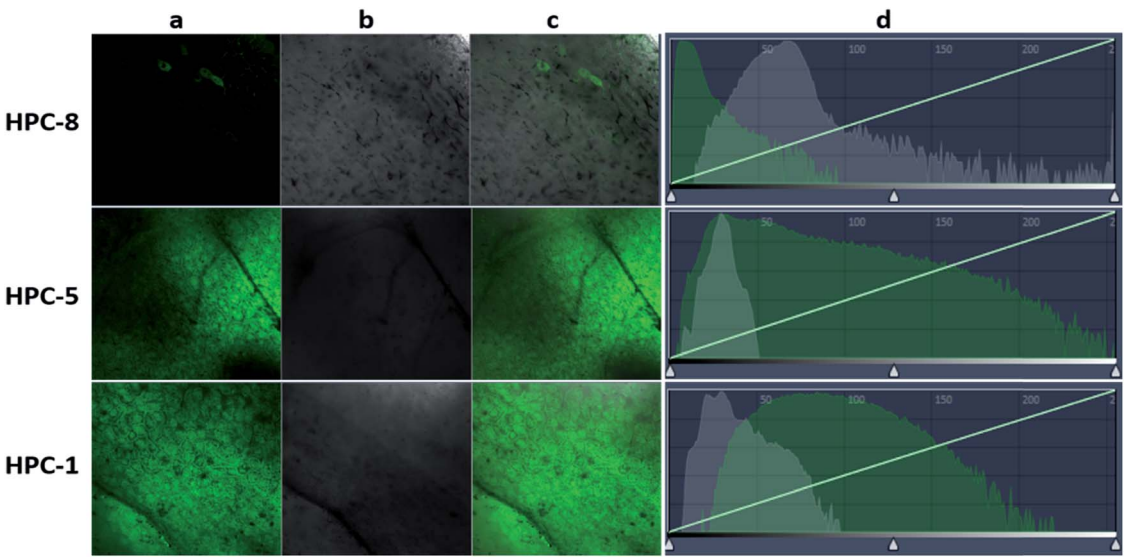

Fig. 8 Cardiac perfusion imaging of probes in the livers of mice. 50 mL (20 μM) samples of **HPC-8**, **HPC-5** and **HPC-1** solutions were respectively injected into the superior vena cava of mice over 10 min at a rate of 2 drops per second, and the livers were dissected for imaging analysis: (a) emission channel (430–650 nm); (b) bright field; (c) merged.

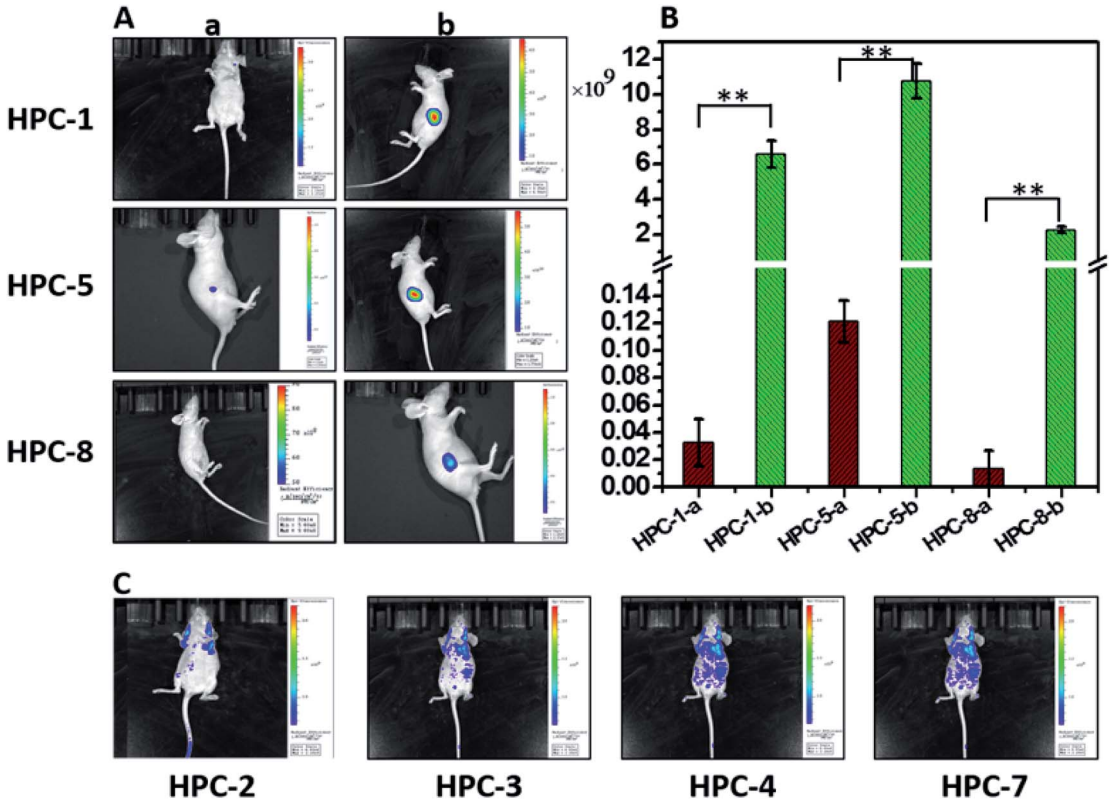

Fig. 9 (A) *In vivo* fluorescence imaging of (a) HPC-*n* and (b) Zn–HPC-*n* (*n*: **1**, **5**, **8**) in mice. (B) Fluorescence intensity collected from (A-a) and (A-b) with statistical analysis performed using Student's *t*-test ($n = 10$), $^{**}P < 0.01$. (C) *In vivo* fluorescence imaging of HPC-**2**, HPC-**3**, HPC-**4** and HPC-**7** in mice. HPC-*n* and Zn–HPC-*n* (100 μL, 20 μM).

from **hpy** to **HPC** in their Zn-coordinated products. As seen from Fig. 7C, with increasing **ESET**, the reporting signals increased. Clearly, **HPC** obtained more electrons at the excited state, which increased the probability of a transition, thereby enhancing the signals. The third group included **HPC-7**, **HPC-8** and **HPC-5**, which led to increased **ESET** from the donor **hpy** to the fluorophore **HPC** (Fig. 7C) with their electron-withdrawing moiety. Accordingly, these compounds exhibited a gradually increased fluorescence intensity. The above described investigations demonstrate that the reporting signal can be obviously regulated by **ESET** although these compounds all comply with the **PET**-inhibited turn on of fluorescence. Thus, we can achieve a probe with a strong reporting intensity by decreasing the **ESET** from **F** to **D** and also forbidding the **PET**. However, in practice, it is still necessary to consider the question of whether to choose a probe with a higher reporting intensity or a greater florescence enhancement. From Fig. 7B and D, it can be seen that **HPC-5** responds to Zn using the strongest fluorescence intensity, but its background fluorescence is not the lowest, and also its fluorescence enhancement is not the largest (70 fold). While, **HPC-1** displayed a lower background and quite a good enhancement of 140 folds, its reporting intensity is not the largest. The same is true for **HPC-8**. Thus, for the *in vivo* imaging, we performed a thorough investigation of the advantages of the fluorescence background (**HPC-8**) and reporting intensity (**HPC-5**), as well as the responding fold increase (**HPC-1**). Prior to the *in vivo* imaging, we investigated these probes in the liver tissues of mice. To ensure the consistency, a saline solution of the probe (**HPC-8**; **HPC-5**; **HPC-1**) was injected into the heart of mice over 10 min at the rate of 2 drops per second, then the liver was dissected for imaging. As Fig. 8 shows, **HPC-5** and **HPC-1** exhibit a stronger fluorescence than **HPC-8**, suggesting that the two are more beneficial to tissue penetration. This result can be confirmed by the fluorescence intensity distribution on the right. Fig. 8d demonstrates that **HPC-5** and **HPC-1** provide the reporting signals that mainly occupy the high intensity area of the fluorescence scale, while **HPC-8** mostly provided the reporting signals in the low-intensity area. Thus, for tissue penetration, a probe that responds with a sufficiently strong intensity should be what we need, and this provides important guidance for the following *in vivo* imaging.

Maximizing the reporting intensity for further reduction of the FNB

Unlike cell or tissue imaging, *in vivo* imaging is more challenging owing to the thick fur and self-fluorescence. Even for near-infrared probes, a high dosage is needed to provide a reporting signal strong enough for penetrating the fur. To overcome this difficulty, we can use this modulation strategy to achieve a probe with a strong intensity, so as to reduce the **FNB** to the lowest level. Therefore, we investigated the probes with both a high reporting intensity and a high sensitivity for their

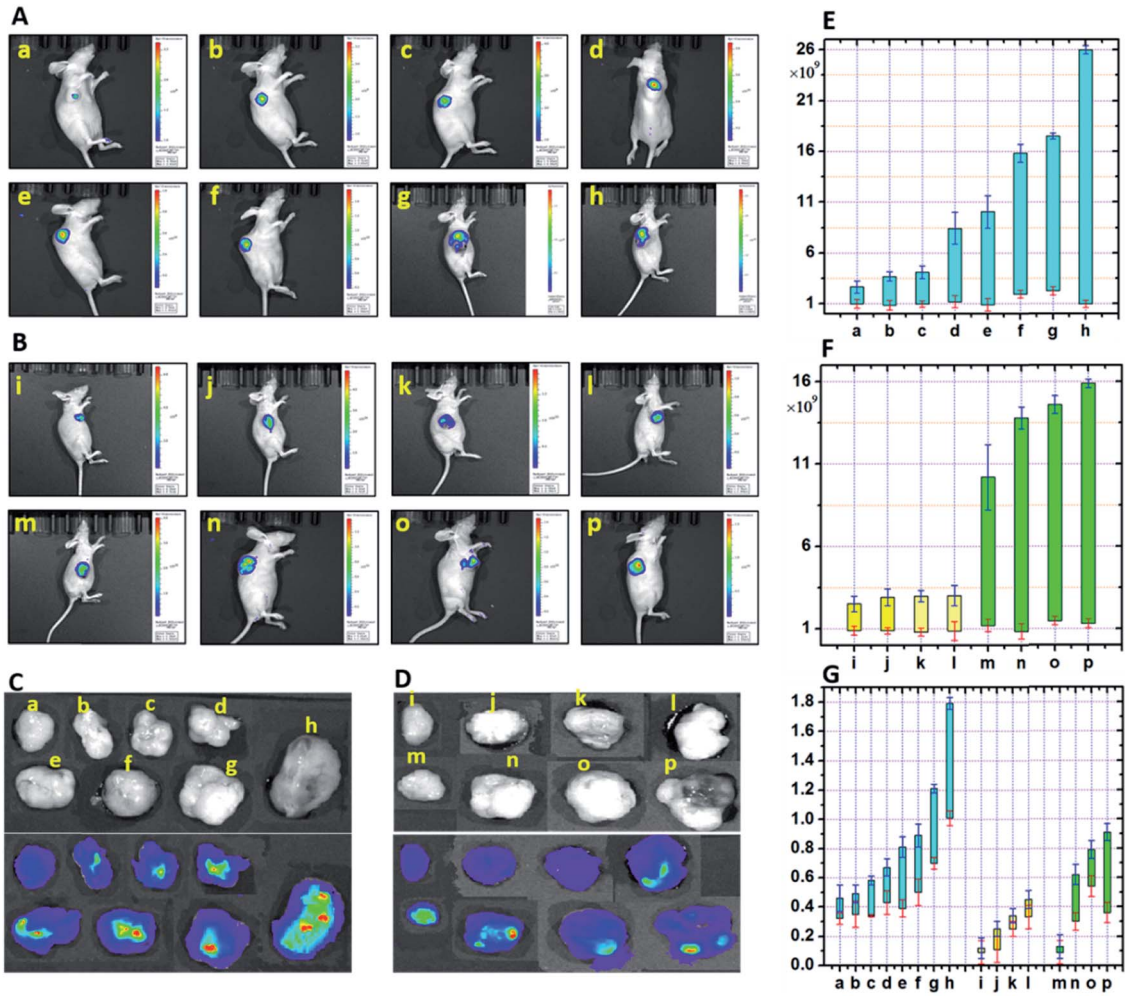

Fig. 10 *In vivo* fluorescence imaging of zinc in mice tumors. (A) 100 μL of zinc chloride solution (**a** to **h**: 0; 10; 30; 60; 100; 150; 200; and 300 μM) was injected into each group for 4 weeks. (B) 100 μL of zinc chloride solution (100 μM) was injected into each group for 4 weeks when tumors were visible to the naked eye (**m**: 1 week; **n**: 2 weeks; **o**: 3 weeks; **p**: 4 weeks); the control group (**i**: 1 week; **j**: 2 weeks; **k**: 3 weeks; **l**: 4 weeks) was injected with physiological saline. (C) Fluorescence imaging of the anatomical tumors from group (A). (D) Fluorescence imaging of the anatomical tumors from group (B). (E) and (F) Fluorescence intensity distributions collected from groups (A) and (B). (G) Weights of the anatomical tumors. **HPC-5** probe (100 μL; 20 μM) was injected before *in vivo* imaging was performed 20 min later. Data are expressed as the mean ± S.D. ($n = 10$).

practicability in *in vivo* imaging. These probes include **HPC-1**, **HPC-2**, **HPC-3**, **HPC-4**, **HPC-5**, **HPC-7** and **HPC-8**, which can offer more than a 50 fold increase in the fluorescent response. As shown in Fig. 9A-a, **HPC-1**, **HPC-5** and **HPC-8** exhibit an insignificant **FNB**. Then, in order to evaluate their reporting intensity, we injected Zn–**HPC-1**, Zn–**HPC-5** and Zn–**HPC-8** into mice. From Fig. 9A-b, it can be observed that Zn–**HPC-8** provided a weak intensity. We list the fluorescence intensity in Fig. 9B, from which we can see that **HPC-5**-b provided the strongest fluorescence. This result indicates that the fluorescent response of **HPC-5** is most likely to be detected during the *in vivo* imaging. Moreover, on the premise of sufficient intensity, we can reduce the dosage of **HPC-5** to further reduce the **FNB**. Although **HPC-1** and **HPC-8** have a lower background, neither of them can provide a stronger reporting intensity than **HPC-5**. It is no doubt that the reporting signal can be displayed by reducing the fluorescence scale of the microscope, but the self-fluorescent background of fur will be passively enhanced. For example, owing to their weak reporting fluorescence intensities, if probes **HPC-2**, **HPC-3**, **HPC-4** and **HPC-7** were to exhibit a detectable reporting signal, without increasing their dosage, the fluorescence scale would have to be decreased. As a result, the fluorescent backgrounds of the probes themselves would be forced to rise, as shown in Fig. 9C. Consequently, for *in vivo* imaging, probe **HPC-5**, which has a high reporting intensity should be competent.

In vivo monitoring of zinc during tumor development

On the basis of the above described investigations, we set out to perform imaging analysis of zinc in tumors to give the first *in vivo* fluorescence imaging of zinc. The role of zinc in tumors has always been subtle. It is reported that the proliferative effect of the growth factor in tumors is accompanied by a zinc increase,

and in the case of zinc deprivation, cell proliferation is reduced.[38] Cancerous cells may accumulate more zinc than juxtaposed non-cancerous cells, implying a potential tissue specificity for zinc distribution. However, fluorescence visualization of this characteristic during tumor development of hepatocellular carcinoma is still challenging. Therefore, we hoped to achieve this with the aid of the probe featuring an ultra-low **FNB** and a strong reporting intensity. First, we investigated the accumulation of zinc at different levels during the development of hepatocellular carcinoma in mice. Mice were subcutaneously inoculated with HepG2 cells, and their growth and tumorigenesis were observed daily. As shown in Fig. 10A, the fluorescence intensity in the blank group **a** was found to be the lowest. The maximum fluorescence intensity was gradually enhanced from group **b** to **h**, which indicated the increased peak value of the Zn accumulated in the tumors. The lowest value for the fluorescence intensity did not exhibit a significant increase, which can be attributed to the metabolic and regulatory effects. This experiment demonstrates that the probe **HPC-5** is sensitive to the rising zinc *in vivo* and can thus be used to monitor zinc-mediated tumor development. Based on this, we then tracked the time-dependent development of tumor-bearing mice. We divided the mice into two groups, respectively, for the control and test. 100 μL of $ZnCl_2$ solution (100 μM) was injected into mice to achieve stable statistical data. *In vivo* imaging was performed during 1–4 weeks of tumor development. From Fig. 10B and F, we observed a significantly strong fluorescence intensity distribution in groups **m** to **p**, compared with the control groups **i** to **l**. Moreover, during the development of the tumor, the fluorescence intensity showed a time-dependent upward trend, indicating the accumulation of zinc in the tissues of the tumor. For confirmation, we analyzed the anatomical tumors. As shown in Fig. 10G, the weight of the tumors from groups **a** to **h** exhibited an upward trend, which was due to the fact that the accumulated zinc led to vigorous cell mitosis and promoted the up-regulation of growth factors. Obviously, the fluorescence intensity of anatomical tumors was positively correlated with the Zn-accumulated development of the hepatocellular carcinoma. Therefore, under the mode of high fidelity, the *in vivo* imaging of Zn accumulation during tumor development was successfully completed.

Conclusions

We have constructed an **F–D–R** system for the cross-talk modulation of **ESET** and **PET**, and thereby *de novo* designed a series of fluorescent probes for high fidelity imaging. These allow: (1) the adjustment of **R** to enhance **ESET** from **F** to **D** on the basis of synergistic **PET** to minimize the inherent **FNB**; and (2) the inhibition of **PET** and the decrease of **ESET** from **F** to **D** to enhance the reporting fluorescence, thereby further minimizing the **FNB**. This strategy allows researchers to design practical probes with minimal backgrounds and maximal reporting signals for high fidelity imaging without false negative responses. Benefiting from this strategy, a negligible **FNB** was achieved in the imaging analysis of cells/zebrafish/tissues, even under the rather low intensity scale of microscopy that can uncover the **FNB**. For the first time, the *in vivo* imaging analysis of zinc accumulation in malignant tumors was performed. This strategy and the implementation of this *de novo* design will provide the methodology to find practical molecular probes for *in vivo* imaging.

Conflicts of interest

There are no conflicts to declare.

Acknowledgements

All experiments were performed in compliance with the Chinese National Standard Laboratory Animal Guidelines for ethical review of animal welfare (GB/T 35892-2018) and all experiments followed institutional guidelines. All protocols were approved by the Institutional Animal Care and Use Committee in Binzhou Medical University, Yantai, China. Approval number: BZ2014-102R. This work was supported by the National Natural Science Foundation of China (No. 21535004, 91753111, 21390411, 21475074, and 21403123), the China Postdoctoral Science Foundation (2017M622254; 2016M600531), the Open Funds of the Shandong Province Key Laboratory of Detection Technology for Tumor Markers (KLDTTM2015-6; KLDTTM2015-9), and the Natural Science Foundation of Shandong Province (ZR201709240033; ZR2019MB016).

Notes and references

1 J. Ning, T. Liu, P. Dong, W. Wang, G. Ge, B. Wang, Z. Yu, L. Shi, X. Tian, X. Huo, L. Feng, C. Wang, C. Sun, J. Cui, T. D. James and X. Ma, *J. Am. Chem. Soc.*, 2019, **141**, 1126–1134.
2 H. Wang, J. Chang, M. Shi, W. Pan, N. Li and B. Tang, *Angew. Chem.*, 2019, **131**, 1069–1073.
3 W. Gao, Y. Sun, M. Cai, Y. Zhao, W. Cao, Z. Liu, G. Cui and B. Tang, *Nat. Commun.*, 2018, **9**, 231.
4 Y. L. Pak, S. J. Park, D. Wu, B. Cheon, H. M. Kim, J. Bouffard and J. Yoon, *Angew. Chem., Int. Ed.*, 2018, **57**, 1567–1571.
5 J. Zhang, X. Chai, X.-P. He, H.-J. Kim, J. Yoon and H. Tian, *Chem. Soc. Rev.*, 2019, **48**, 683–722.
6 D. Cheng, J. Peng, Y. Lv, D. Su, D. Liu, M. Chen, L. Yuan and X. Zhang, *J. Am. Chem. Soc.*, 2019, **141**, 6352–6361.
7 N. Sun, D. Malide, J. Liu, I. I. Rovira, C. A. Combs and T. Finkel, *Nat. Protoc.*, 2017, **12**, 1576–1587.
8 Z. Ye, H. Yu, W. Yang, Y. Zheng, N. Li, H. Bian, Z. Wang, Q. Liu, Y. Song, M. Zhang and Y. Xiao, *J. Am. Chem. Soc.*, 2019, **141**, 6527–6536.
9 J. Shin, P. Verwilst, H. Choi, S. Kang, J. Han, N. H. Kim, J. G. Choi, M. S. Oh, J. S. Hwang, D. Kim, I. Mook-Jung and J. S. Kim, *Angew. Chem.*, 2019, **131**, 5704–5708.
10 X. Wu, W. Shi, X. Li and H. Ma, *Acc. Chem. Res.*, 2019, **52**, 1892–1904.
11 P. Mouroulis and R. O. Green, *Opt. Eng.*, 2018, **57**, 1–19.
12 J. Zhang, Q. Wang, Z. Guo, S. Zhang, C. Yan, H. Tian and W.-H. Zhu, *Adv. Funct. Mater.*, 2019, **29**, 1808153.

13 J. Ning, W. Wang, G. Ge, P. Chu, F. Long, Y. Yang, Y. Peng, L. Feng, X. Ma and T. D. James, *Angew. Chem., Int. Ed.*, 2019, **58**, 9959–9963.
14 W. Fu, C. Yan, Z. Guo, J. Zhang, H. Zhang, H. Tian and W.-H. Zhu, *J. Am. Chem. Soc.*, 2019, **141**, 3171–3177.
15 Y. Yang, S. K. Seidlits, M. M. Adams, V. M. Lynch, C. E. Schmidt, E. V. Anslyn and J. B. Shear, *J. Am. Chem. Soc.*, 2010, **132**, 13114–13116.
16 H. Kobayashi, M. Ogawa, R. Alford, P. L. Choyke and Y. Urano, *Chem. Rev.*, 2010, **110**, 2620–2640.
17 H. S. Choi, S. L. Gibbs, J. H. Lee, S. H. Kim, Y. Ashitate, F. Liu, H. Hyun, G. Park, Y. Xie, S. Bae, M. Henary and J. V. Frangioni, *Nat. Biotechnol.*, 2013, **31**, 148–153.
18 L. Lauinger, J. Li, A. Shostak, I. A. Cemel, N. Ha, Y. Zhang, P. E. Merkl, S. Obermeyer, N. Stankovic-Valentin, T. Schafmeier, W. J. Wever, A. A. Bowers, K. P. Carter, A. E. Palmer, H. Tschochner, F. Melchior, R. J. Deshaies, M. Brunner and A. Diernfellner, *Nat. Chem. Biol.*, 2017, **13**, 709–714.
19 E. B. Wright and T. L. Dormandy, *Nature*, 1972, **237**, 166.
20 N. W. H. Addink, *Nature*, 1950, **166**, 693.
21 P. A. Futreal, L. Coin, M. Marshall, T. Down, T. Hubbard, R. Wooster, N. Rahman and M. R. Stratton, *Nat. Rev. Cancer*, 2004, **4**, 177–183.
22 K. Komatsu, K. Kikuchi, H. Kojima, Y. Urano and T. Nagano, *J. Am. Chem. Soc.*, 2005, **127**, 10197–10204.
23 M. Royzen, A. Durandin, V. G. Young, N. E. Geacintov and J. W. Canary, *J. Am. Chem. Soc.*, 2006, **128**, 3854–3855.
24 K. Kiyose, H. Kojima, Y. Urano and T. Nagano, *J. Am. Chem. Soc.*, 2006, **128**, 6548–6549.
25 F. Qian, C. Zhang, Y. Zhang, W. He, X. Gao, P. Hu and Z. Guo, *J. Am. Chem. Soc.*, 2009, **131**, 1460–1468.
26 G. Masanta, C. S. Lim, H. J. Kim, J. H. Han, H. M. Kim and B. R. Cho, *J. Am. Chem. Soc.*, 2011, **133**, 5698–5700.
27 Z. Guo, G.-H. Kim, J. Yoon and I. Shin, *Nat. Protoc.*, 2014, **9**, 1245–1254.
28 D. Li, S. Chen, E. A. Bellomo, A. I. Tarasov, C. Kaut, G. A. Rutter and W.-h. Li, *Proc. Natl. Acad. Sci. U. S. A.*, 2011, **108**, 21063–21068.
29 Z. Liu, C. Zhang, Y. Chen, W. He and Z. Guo, *Chem. Commun.*, 2012, **48**, 8365–8367.
30 C. Zhang, Z. Liu, Y. Li, W. He, X. Gao and Z. Guo, *Chem. Commun.*, 2013, **49**, 11430–11432.
31 P. Du and S. J. Lippard, *Inorg. Chem.*, 2010, **49**, 10753–10755.
32 J. E. Kwon, S. Lee, Y. You, K.-H. Baek, K. Ohkubo, J. Cho, S. Fukuzumi, I. Shin, S. Y. Park and W. Nam, *Inorg. Chem.*, 2012, **51**, 8760–8774.
33 B. Tang, H. Huang, K. Xu, L. Tong, G. Yang, X. Liu and L. An, *Chem. Commun.*, 2006, 3609–3611, DOI: 10.1039/b606809j.
34 Z. Xu, J. Yoon and D. R. Spring, *Chem. Soc. Rev.*, 2010, **39**, 1996–2006.
35 Y. Chen, Y. Bai, Z. Han, W. He and Z. Guo, *Chem. Soc. Rev.*, 2015, **44**, 4517–4546.
36 W. Li, B. Fang, M. Jin and Y. Tian, *Anal. Chem.*, 2017, **89**, 2553–2560.
37 A. M. Hessels, P. Chabosseau, M. H. Bakker, W. Engelen, G. A. Rutter, K. M. Taylor and M. Merkx, *ACS Chem. Biol.*, 2015, **10**, 2126–2134.
38 Y. Cui, S. Vogt, N. Olson, A. G. Glass and T. E. Rohan, *Cancer Epidemiol., Biomarkers Prev.*, 2007, **16**, 1682–1685.